

# Neural Networks for Full Phase-space Reweighting and Parameter Tuning

Anders Andreassen<sup>1,2,\*</sup> and Benjamin Nachman<sup>2,†</sup>

<sup>1</sup>*Department of Physics, University of California, Berkeley, CA 94720, USA*

<sup>2</sup>*Physics Division, Lawrence Berkeley National Laboratory, Berkeley, CA 94720, USA*

Precise scientific analysis in collider-based particle physics is possible because of complex simulations that connect fundamental theories to observable quantities. The significant computational cost of these programs limits the scope, precision, and accuracy of Standard Model measurements and searches for new phenomena. We therefore introduce *Deep neural networks using Classification for Tuning and Reweighting* (DCTR), a neural network-based approach to reweight and fit simulations using the full phase space. DCTR can perform tasks that are currently not possible with existing methods, such as estimating non-perturbative fragmentation uncertainties. The core idea behind the new approach is to exploit powerful high-dimensional classifiers to reweight phase space as well as to identify the best parameters for describing data. Numerical examples from  $e^+e^- \rightarrow \text{jets}$  demonstrate the fidelity of these methods for simulation parameters that have a big and broad impact on phase space as well as those that have a minimal and/or localized impact. The high fidelity of the full phase-space reweighting enables a new paradigm for simulations, parameter tuning, and model systematic uncertainties across particle physics and possibly beyond.

In collider-based high-energy physics, detector simulations and parton shower Monte Carlo (MC) programs enable scientific inference by connecting fundamental theories to observable quantities. However, these tools are often computationally slow and emulate probability distributions that are analytically intractable. This has resulted in three key simulation challenges for the particle physics community: (1) an insufficient number of simulated events, (2) unaccounted for biases from simulation parameters, and (3) the inability to utilize the full phase space for parameter tuning.

A variety of approaches have been proposed to address the above challenges. The two existing solutions to (1) are to use more [1–4] or faster computers or accelerators [5, 6] or to build fast surrogate models (‘fast simulation’). Machine learning tools hold great promise for augmenting [7] or replacing [8–21] current fast simulation approaches, but are not yet precise enough to match full, physics-based simulators. Deep learning methods to circumvent expensive simulations for hypothesis testing were studied in the context of effective field theory fits [22–24]; related ideas will be useful also for reweighting. The only solution for (2) aside from generating a large set of simulations is to assign event weights for parameter variations. Currently, this is only possible for a small number of perturbative parameters in parton shower programs [25–27] and for parton distribution functions [28, 29]. Pseudo-automated procedures exist for tuning parton shower models [30, 31], but the format of the existing public data means that these algorithms are restricted to a set of one-dimensional inputs that must be assumed to be independent.

This letter introduces *Deep neural networks using Classification for Tuning and Reweighting* (DCTR, pronounced “doctor”), a new approach to solve all three computational challenges. In particular, deep neural network-based classifiers are used to (continuously)

reweight one particle-level simulation into another and additionally use the full phase space to fit parameters within a given model. Non-deep machine learning tools have been used in the past for discrete reweighting [19, 32–34] with a small number of observables. Deep-learning-based discrete weighting was considered in [19, 35] and continuous single observable reweightings were presented in [36]. The re-weighting presented here combines a full-phase space deep learning architecture [37] with parameterization [38] to fully morph one simulation into another. There are no restrictions on the size of the input feature space nor on the number of interpolated parameters. In addition to re-weighting, we show how DCTR can be used with a differentiable re-weighting function (such as the one just mentioned) to optimize simulation parameters. This fitting procedure uses a classifier as a loss function, which can readily incorporate all of the information from the (potentially high-dimensional) input features.

The first ingredient to the full phase-space reweighting procedure is a prescription to derive event weights. Consider two simulations that describe the same phase space  $\Omega$  and are described by probability densities  $p_0(x)$  and  $p_1(x)$ , for  $x \in \Omega$ . Assuming that  $p_0$  and  $p_1$  have the same support, the function  $w(x) = p_0(x)/p_1(x)$  is the ideal per-event weight to morph the second simulation into the first one. A key observation made by multiple groups in the past is that  $w$  can be well-approximated by training a machine learning classifier to distinguish the two simulations. For example, let  $f(x)$  be parameterized by a neural network and trained with the binary cross-entropy loss:

$$\text{loss}(f(x)) = - \sum_{i \in \mathbf{0}} \log f(x_i) - \sum_{i \in \mathbf{1}} \log(1 - f(x_i)), \quad (1)$$

where  $\mathbf{0}$  and  $\mathbf{1}$  represent sets of examples from the

two simulations. Then a well-known result is that<sup>1</sup>,  $f(x)/(1-f(x)) \approx p_0(x)/p_1(x)$ . The benefit of parameterizing  $f$  as a neural network is that deep learning can readily analyze all of  $\Omega$ , which was not possible with shallow learning attempts with a similar statistical foundation. The closest attempt to a full phase space approach directly tried to learn  $p_i(x)$  using the full kinematic (i.e. non-flavor) part of  $\Omega$  [35], but this is much harder than learning the ratio.

An important reweighting scenario is when the two simulations are from the same simulation program, but with different model parameters,  $\theta$ . For example, when model uncertainties are evaluated, one may want to transform  $p_\theta(x)$  into  $p_{\theta+\delta_\theta}(x)$ . When these uncertainties are profiled in a fit, it is important that the transformation procedure be able to continuously interpolate between model parameters. The neural network reweighting approximation can be extended to this continuous case by adding  $\theta$  as a feature [38]:  $f(x, \theta)$ . In the examples presented below, the training data are generated with a uniform distribution in  $\theta$ , but this probability density can be optimized per application and can even be discrete.

Even though simulators have many parameters that must be fit to data, gradient methods cannot be used directly with the models as they are non-differentiable. Surrogate generative models built from neural networks can be used for gradient-based parameter fitting, but may not have sufficient quality to be reliable. Reweighting is a robust alternative to surrogate generative models. A neural network-based continuous reweighting function is essentially a differentiable (in model parameters) version of the original simulator and can be used to perform inference on the parameters themselves. This is especially powerful for particle-level parameter tuning to data where one sample with a computationally expensive full detector simulation can be continuously reweighted to other parameter points with the same detector model at no extra simulation cost.

An ideal loss function used to fit model parameters makes use of the full observable phase space. Typical metrics such as the  $\chi^2$  between histogram approximations to probability densities become impractical when  $\Omega$  is high dimensional. As described above, classifiers are powerful tools for accessing all of the available information. Therefore, one can use a classifier *for the loss*. When a classifier trained to distinguish some  $\theta_0$  from a  $\theta_1$  performs poorly, then the two samples are close. While using classification to quantify differences between event samples has been used for anomaly detection [39–41], we are unaware of an example where it is used for parameter fitting. The idea of using the classifier loss as a metric is

similar to the minimax strategy in Generative Adversarial Networks [42], only in this context the generative part is a reweighter and is trained independently. A more elegant way of implementing this approach is to fit unknown parameters to the values that minimize the nominal classifier loss. In particular, suppose that a reweighter neural network  $f$  is trained as described above. Such a function will satisfy

$$f(x, \theta) = \operatorname{argmax}_{f'} \sum_{i \in \theta_0} \log f'(x_i, \theta) + \sum_{i \in \theta} \log(1 - f'(x_i, \theta)) \quad (2)$$

for all  $\theta$ . Note that the  $f'$  in the first sum takes the parameter  $\theta$  and not  $\theta_0$ , otherwise the discrimination task would be trivial. Now, suppose there is a new sample  $\theta_1$  where  $\theta_1$  is unknown (for instance,  $\theta_1$  are collider data). The claim is that if  $\theta^*$  is chosen as

$$\theta^* = \operatorname{argmax}_{\theta'} \sum_{i \in \theta_0} \log f(x_i, \theta') + \sum_{i \in \theta_1} \log(1 - f(x_i, \theta')) \quad (3)$$

then  $\theta^* = \theta_1$ . As  $f$  minimizes the cross-entropy loss for any  $\theta$  (Eq. 2),

$$\begin{aligned} & \sum_{i \in \theta_0} \log f(x_i, \theta_1) + \sum_{i \in \theta_1} \log(1 - f(x_i, \theta_1)) \\ & \geq \sum_{i \in \theta_0} \log f(x_i, \theta^*) + \sum_{i \in \theta_1} \log(1 - f(x_i, \theta^*)) \end{aligned} \quad (4)$$

must hold. However, the converse must also be true since  $\theta^*$  minimizes the cross-entropy loss as well and therefore,  $\theta^* = \theta_1$ . Since  $f$  is differentiable, Eq. 3 can be solved using standard gradient-based methods.

The last ingredient to DCTR is a suitable neural network architecture that can effectively capture all the salient features of  $\Omega$ . A natural tool for this task is the Particle Flow Network (PFN) [37], built on the Deep Sets framework [43]. While many deep learning architectures incorporate the symmetries and structure of high energy physics events [9, 35, 44–54], PFNs are particularly effective because they can operate on variable-length sets of particles and respect the quantum-mechanically induced permutation invariance of particle labels. These networks can also readily incorporate non-kinematic information such as particle flavor. A particle flow network is a composition of two neural networks  $F$  and  $\Phi$ :  $f(\{p_i\}) = F(\sum_{i=1}^n \Phi(p_i))$ , where  $p_i$  is the set of features belong to particle  $i$  (momentum and flavor) as well as  $\theta$ . The function  $\Phi$  embeds the input particles into an  $\ell$ -dimensional *latent space* and  $F$  is a simple  $\mathbb{R}^\ell \mapsto \mathbb{R}$  neural network. References [37, 43] proved that this structure is sufficiently flexible to approximate any function and in practice,  $\ell \sim \mathcal{O}(10)$ .

To illustrate the potential of DCTR, full phase-space reweighting and parameter tuning is performed on a sample of simulated events from the PYTHIA 8.230 [55, 56]

<sup>1</sup> See Appendix A for the derivation.

event generator. Particle-level  $e^+e^- \rightarrow Z \rightarrow$  dijet events with about 100 particles in each event are clustered into jets using the anti- $k_t$  clustering algorithm [57] ( $R = 0.8$ ) with Fastjet 3.0.3 [58, 59]. The jets are presented to the neural network for training, with each jet constituent represented by  $(p_T, \eta, \phi, \text{particle type}, \theta)$ , where  $\theta$  is the parameter in Eq. (2). One million events were generated for each set of PYTHIA parameters. In addition to a default parameter set using the Monash tune [60], three separate samples were generated with uniformly sampled `TimeShower:alphaSvalue`, `StringZ:aLund` and `StringFlav:probStoUD` in the ranges  $[0.10, 0.18]$ ,  $[0.50, 0.90]$  and  $[0.10, 0.30]$ , respectively. We also generated one sample where all three parameters were simultaneously uniformly sampled. These parameters were chosen because they represent both perturbative and non-perturbative physical effects and the ranges are similar to those studied in Ref. [31]. The Monash values of the three parameters are 0.1365, 0.68, and 0.217, respectively.

The reweighting and fitting was found to work well without any hyperparameter modifications from Ref. [37]. In particular,  $\Phi$  has two hidden layers with  $\ell = 128$  and  $F$  is composed of three hidden layers and two output nodes for binary classification, and all the hidden layers have 100 nodes. The activation function used for all layers is ReLU with the exception of the classification output which uses softmax. All models were implemented in Keras [61] with the Tensorflow backend [62] and trained using the crossentropy loss with the Adam [63] optimizer for 50 epochs, using early stopping with patience 10, with batch size 1000. Each training set contained  $8 \cdot 10^5$  training and  $10^5$  validation jets of each class. Training time was 10-15 min for each model (20 seconds per epoch) on an NVIDIA GeForce GTX 1080.

As a first test of DCTR, a single parameter (`TimeShower:alphaSvalue`) is reweighted using the full phase space of the simulated jets. Results for discrete and continuous reweighting from a varied parameter to the nominal sample are presented in Fig. 1. The entire phase-space is reweighted, but is too high dimensional to visualize. Instead, three histograms of physically relevant one-dimensional observables are presented: the number of particles inside the jet (multiplicity), an  $n$ -subjettiness ratio  $\tau_{32}$  [64, 65], and a four-point Energy Correlation Function [66]  $\text{ECF}(N = 4, \beta = 4)$ . By definition,  $\tau_{32} = \tau_3/\tau_2$  where  $\tau_n = \sum_{i \in \text{jet}} p_{T,i} \min_{j=1 \dots n} \{\Delta R(i, j)\}$  for axis  $j$ ; likewise,  $\text{ECF}(N, \beta)$  is the sum over all quadruples inside the jet weighted by the product of the momenta and the product of all opening angles raised to the power  $\beta$ . The large values of  $n$ ,  $N$ , and  $\beta$  are used to expose complex features with a nontrivial dependence on all particles inside the jet. Many more observables were studied, but these ones are representative.

The reweighted distributions are in excellent agreement with the target nominal distribution.

Samples used to make the histograms shown for `TimeShower:alphaSvalue` values 0.1365 and 0.1600 were not used during training or validation. The fidelity of a continuous reweighting is quantified in the lower right plot of Fig. 1, which presents the  $\chi^2/\text{ndf}$  as a function of the initial  $\alpha_s$  parameter value.

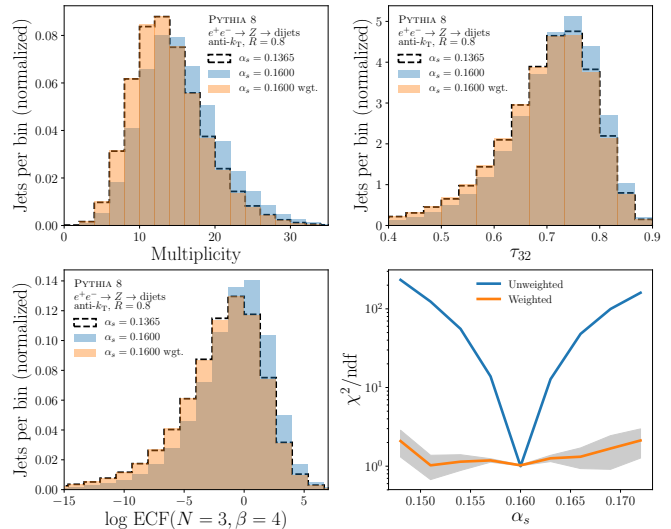


FIG. 1. The three histograms shows the result before and after reweighting between two values of `TimeShower:alphaSvalue` =  $\alpha_s$  on different 1D observables. To quantify the quality of the reweighting, and to illustrate one trained model can continuously reweight for any parameter, we show the  $\chi^2/\text{ndf}$  as a function of  $\alpha_s$  in the lower right plot. For each value, we compare the  $\chi^2$  relative to  $\alpha_s = 0.1600$  before and after reweighting. Each  $\chi^2$  value is averaged over 10 runs and the grey band marks the standard deviation, which is consistent with  $\chi^2/\text{ndf} \approx 1$ .

Variations in `TimeShower:alphaSvalue` modify many aspects of jet fragmentation and therefore it may be an easy parameter for the reweighting network to learn. In contrast, the hadronization parameters `StringZ:aLund` and `StringFlav:probStoUD` may be more difficult because the size of their effects on the phase space is small and/or localized. Figure 2 shows that despite these potential challenges, the reweighting procedure is able to effectively capture subtle and isolated modifications to the phase space. Variations in the `StringZ:aLund` parameter result in mostly percent-level differences in the presented distributions, which are corrected in the reweighted model. Modifying the `StringFlav:probStoUD` parameter only changes strange particles such as kaons, which highlights the importance of including flavor in the full phase space network. Importantly, this model learns to only change the distributions related to strange particles, leaving other observables untouched. Simultaneously reweighting all three parameters also works well, but is more difficult to visualize. We also verified that DCTR works for  $pp$  MC simulations by reweighting from

PYTHIA to HERWIG for both the quark and gluon samples taken from [37, 67, 68].

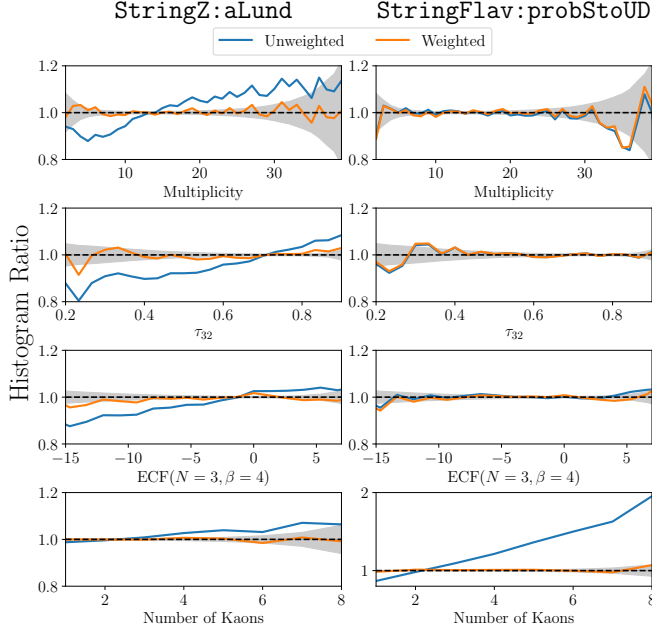


FIG. 2. Ratio of histograms from nominal distribution to sample generated with `StringZ:aLund` = 0.8 on the left and `StringFlav:probStoUD` = 0.275 on the right. Both unweighted and weighted histograms ratios are shown. The gray band indicates the statistical uncertainty from both the nominal and variation sample. After reweighting, the ratio only differs from 1 within the statistical uncertainty.

The well-trained DCTR model can now be used to demonstrate the potential for parameter tuning following Eq. 3. As a first step, Table I presents the result of a fit where the ‘data’ are the same as the nominal, but with each parameter changed one at a time (each row is a separate fit). To illustrate the sensitivity to the randomness in the model initialization, each fit is performed ten times. This variation could be reduced with a more sophisticated neural network and/or more training data. For each of these one-dimensional fits, the fitted value is consistent with the target value within these statistical fluctuations from initialization, which are 1 – 3%. As `TimeShower:alphaSvalue` has a bigger impact on the phase space, it is less sensitive to the initialization statistical fluctuations.

As a next step, the top part of Table II shows the result of a simultaneous fit to the three parameters. As with the one-dimensional fit, the fitted values are all statistically consistent with the target values. Interestingly, the sensitivity to the initialization statistical fluctuations is about the same for the three-dimensional fit as for the one-dimensional fits, providing confidence in the scaling to more parameters. In practice, the fitting procedure would be validated on a variety of simulations with

TABLE I. Independent fit for simulation where one parameter was changed at a time. The reported numbers are the mean and standard deviation over 10 runs with different model initializations.

Parameter	Target value	Fit value
<code>TimeShower:alphaSvalue</code>	0.1600	$0.1601 \pm 0.0018$
<code>StringZ:aLund</code>	0.8000	$0.7980 \pm 0.0257$
<code>StringFlav:probStoUD</code>	0.2750	$0.2754 \pm 0.0065$

known parameters, as just described. An illustration of the fit itself is shown in Fig. 3, where a two-dimensional slice through the likelihood landscape is presented and the fit execution demonstrated with markers and dashed lines. The broadness of the loss in the `StringZ:aLund` direction relative to the `TimeShower:alphaSvalue` one is a reflection of the significantly smaller impact of fragmentation function variations on the observable phase space compared with modifications to the final state shower strong coupling. After the validation, the model can be deployed on data, where the parameters are unknown. The lower part of Table II replicates this scenario, where the Pythia parameters were blinded during the fit. This closure test indicates that the method is robust to user-bias.

TABLE II. Simultaneous fit for three parameters. The top row shows the results for the validation fit where we knew the target parameters, and the bottom row is the blinded fit. The reported numbers are the mean and standard deviation over 20 runs with different model initializations.

	Parameter	Target value	Fit value
Val.	<code>TimeShower:alphaSvalue</code>	0.1200	$0.1195 \pm 0.0022$
	<code>StringZ:aLund</code>	0.6000	$0.6276 \pm 0.0373$
	<code>StringFlav:probStoUD</code>	0.1200	$0.1203 \pm 0.0071$
Blinded	<code>TimeShower:alphaSvalue</code>	0.1700	$0.1707 \pm 0.0022$
	<code>StringZ:aLund</code>	0.7500	$0.7425 \pm 0.0453$
	<code>StringFlav:probStoUD</code>	0.1400	$0.1422 \pm 0.0065$

The empirical results demonstrate that DCTR is ready to be deployed. The discrete reweighting could be used to generate new full-detector simulated samples with a different particle-level simulation when at least one other fully simulated sample already exists. This could be particularly useful for systematic uncertainties computed using pairs of simulations (e.g. comparing Pythia and Herwig) and for legacy data analysis in which the original detector simulation is no longer available [69]. Continuous reweighting will enable systematic parameter variations for uncertainty estimation that were not possible before (most parameters). Such variations can even be profiled during any statistical test that fits phase space regions



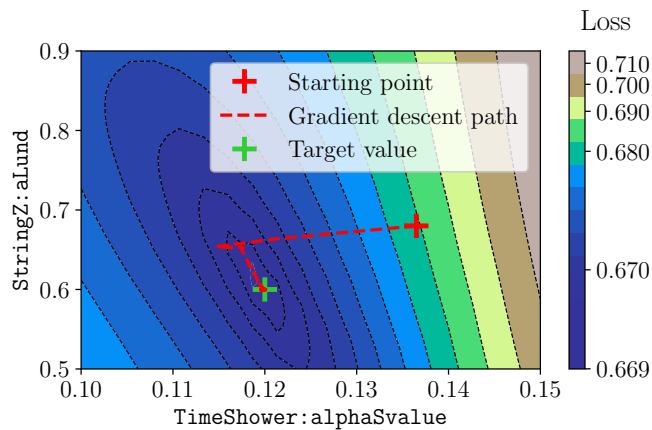


FIG. 3. Two-dimensional slice through the loss surface for the fit described in Table II. Markers indicate the starting point at nominal values, the gradient descent path and the target values. From the starting point, gradient descent using Adam overshoots the minimum in its first two epochs before it converges to the target value.

sensitive to the varied nuisance parameters. Finally, the full power of DCTR can be used for parameter tuning. Unlike traditional tuning which must use unfolded data that are usually one-dimensional and without observable-observable correlations, a new paradigm is now possible where high-dimensional detector-level data can be used directly. The full power of the data can be utilized and all of the correlations are correctly accounted for in the fit. For the first time, this may allow for proper covariance matrices (and thus correlated uncertainties) to be determined for simulation parameter values. All of these opportunities illustrate the broad applicability of full phase-space reweighting and parameter tuning and the power DCTR to extend the scope, precision, and accuracy of collider-based particle physics analyses.

BN would like to thank Luke de Oliveira, Michela Paganini, Chase Shimmin, and Paul Tipton for collaboration on an early stage prototype of this project. We thank Steve Mrenna and Peter Skands for helpful discussions about automated variations in Pythia. We also thank Jesse Thaler, Eric Metodiev, Patrick Komiske, Aviv Cukierman for lively discussions about deep learning-based reweighting. This work was supported by the U.S. Department of Energy, Office of Science under contract DE-AC02-05CH11231. Finally, we are grateful for the opportunity to use the Cori supercomputing resources at NERSC.

\* andersja@berkeley.edu

† bpnachman@lbl.gov

[1] S. Ahn, J. Apostolakis, M. Asai, D. Brandt, G. Cooperman, G. Cosmo, A. Dotti, X. Dong, S. Yung Jun, and

- A. Nowak (2014) p. 04213.
- [2] S. Farrell, A. Dotti, M. Asai, P. Calafiura, and R. Monnard, in *Proceedings, 2015 IEEE Nuclear Science Symposium and Medical Imaging Conference (NSS/MIC 2015): San Diego, California, United States* (2016) p. 7581868, arXiv:1605.08371 [physics.comp-ph].
- [3] J. T. Childers, T. D. Uram, T. J. LeCompte, M. E. Papka, and D. P. Benjamin, *Comput. Phys. Commun.* **210**, 54 (2017), arXiv:1511.07312 [hep-ph].
- [4] S. Hoche, S. Prestel, and H. Schulz, (2019), arXiv:1905.05120 [hep-ph].
- [5] O. Seiskari, J. Kommeri, and T. Niemi, (2012), arXiv:1209.5235 [physics.comp-ph].
- [6] P. Canal, D. Elvira, S. Y. Jun, J. Kowalkowski, M. Paterno, and J. Apostolakis, *Proceedings, 20th International Conference on Computing in High Energy and Nuclear Physics (CHEP 2013): Amsterdam, The Netherlands, October 14-18, 2013*, *J. Phys. Conf. Ser.* **513**, 052013 (2014).
- [7] ATLAS Collaboration, *ATL-SOFT-PUB-2018-002* (2018).
- [8] M. Paganini, L. de Oliveira, and B. Nachman, *Phys. Rev.* **D97**, 014021 (2018), arXiv:1712.10321 [hep-ex].
- [9] L. de Oliveira, M. Paganini, and B. Nachman, *Comput. Softw. Big Sci.* **1**, 4 (2017), arXiv:1701.05927 [stat.ML].
- [10] M. Paganini, L. de Oliveira, and B. Nachman, *Phys. Rev. Lett.* **120**, 042003 (2018), arXiv:1705.02355 [hep-ex].
- [11] L. de Oliveira, M. Paganini, and B. Nachman, *Proceedings, 18th International Workshop on Advanced Computing and Analysis Techniques in Physics Research (ACAT 2017): Seattle, WA, USA, August 21-25, 2017*, *J. Phys. Conf. Ser.* **1085**, 042017 (2018), arXiv:1711.08813 [hep-ex].
- [12] M. Erdmann, L. Geiger, J. Glombitza, and D. Schmidt, *Comput. Softw. Big Sci.* **2**, 4 (2018), arXiv:1802.03325 [astro-ph.IM].
- [13] P. Musella and F. Pandolfi, *Comput. Softw. Big Sci.* **2**, 8 (2018), arXiv:1805.00850 [hep-ex].
- [14] M. Erdmann, J. Glombitza, and T. Quast, *Comput. Softw. Big Sci.* **3**, 4 (2019), arXiv:1807.01954 [physics.ins-det].
- [15] F. Carminati, A. Gheata, G. Khattak, P. Mendez Lorenzo, S. Sharan, and S. Vallecorsa, *Proceedings, 18th International Workshop on Advanced Computing and Analysis Techniques in Physics Research (ACAT 2017): Seattle, WA, USA, August 21-25, 2017*, *J. Phys. Conf. Ser.* **1085**, 032016 (2018).
- [16] V. Chekalina, E. Orlova, F. Ratnikov, D. Ulyanov, A. Ustyuzhanin, and E. Zakharov, in *23rd International Conference on Computing in High Energy and Nuclear Physics (CHEP 2018) Sofia, Bulgaria, July 9-13, 2018* (2018) arXiv:1812.01319 [physics.data-an].
- [17] B. Hashemi, N. Amin, K. Datta, D. Olivito, and M. Pierini, (2019), arXiv:1901.05282 [hep-ex].
- [18] R. Di Sipio, M. Fucci Giannelli, S. Ketabchi Haghighat, and S. Palazzo, (2019), arXiv:1903.02433 [hep-ex].
- [19] R. Aaij *et al.* (LHCb Collaboration), *Phys. Rev. Lett.* **119**, 062001 (2017), arXiv:1704.07900 [hep-ex].
- [20] J. W. Monk, *JHEP* **12**, 021 (2018), arXiv:1807.03685 [hep-ph].
- [21] ATLAS Collaboration, *ATL-SOFT-PUB-2018-001* (2018).
- [22] J. Brehmer, K. Cranmer, G. Louppe, and J. Pavez, *Phys. Rev. Lett.* **121**, 111801 (2018), arXiv:1805.00013 [hep-

- ph].
- [23] J. Brehmer, K. Cranmer, G. Louppe, and J. Pavez, *Phys. Rev. D* **98**, 052004 (2018), [arXiv:1805.00020 \[hep-ph\]](#).
  - [24] J. Brehmer, G. Louppe, J. Pavez, and K. Cranmer, (2018), [arXiv:1805.12244 \[stat.ML\]](#).
  - [25] S. Mrenna and P. Skands, *Phys. Rev. D* **94**, 074005 (2016), [arXiv:1605.08352 \[hep-ph\]](#).
  - [26] J. Bellm, S. Plätzer, P. Richardson, A. Sidmök, and S. Webster, *Phys. Rev. D* **94**, 034028 (2016), [arXiv:1605.08256 \[hep-ph\]](#).
  - [27] E. Bothmann, M. Schnherr, and S. Schumann, *Eur. Phys. J. C* **76**, 590 (2016), [arXiv:1606.08753 \[hep-ph\]](#).
  - [28] J. Butterworth *et al.*, *J. Phys. G* **43**, 023001 (2016), [arXiv:1510.03865 \[hep-ph\]](#).
  - [29] A. Buckley, J. Ferrando, S. Lloyd, K. Nordström, B. Page, M. Rfenacht, M. Schnherr, and G. Watt, *Eur. Phys. J. C* **75**, 132 (2015), [arXiv:1412.7420 \[hep-ph\]](#).
  - [30] A. Buckley, H. Hoeth, H. Lackner, H. Schulz, and J. E. von Seggern, *The European Physical Journal C* **65**, 331 (2009).
  - [31] P. Ilten, M. Williams, and Y. Yang, *Journal of Instrumentation* **12**, P04028 (2017).
  - [32] D. Martschei, M. Feindt, S. Honc, and J. Wagner-Kuhr, *Proceedings, 14th International Workshop on Advanced Computing and Analysis Techniques in Physics Research (ACAT 2011): Uxbridge, UK, September 5-9, 2011*, *J. Phys. Conf. Ser.* **368**, 012028 (2012).
  - [33] A. Rogozhnikov, *Proceedings, 17th International Workshop on Advanced Computing and Analysis Techniques in Physics Research (ACAT 2016): Valparaíso, Chile, January 18-22, 2016*, *J. Phys. Conf. Ser.* **762**, 012036 (2016), [arXiv:1608.05806 \[physics.data-an\]](#).
  - [34] M. Aaboud *et al.* (ATLAS Collaboration), *Phys. Rev. D* **98**, 092002 (2018), [arXiv:1806.04030 \[hep-ex\]](#).
  - [35] A. Andreassen, I. Feige, C. Frye, and M. D. Schwartz, (2018), [arXiv:1804.09720 \[hep-ph\]](#).
  - [36] E. Bothmann and L. Debbio, *JHEP* **01**, 033 (2019), [arXiv:1808.07802 \[hep-ph\]](#).
  - [37] P. T. Komiske, E. M. Metodiev, and J. Thaler, *JHEP* **01**, 121 (2019), [arXiv:1810.05165 \[hep-ph\]](#).
  - [38] P. Baldi, K. Cranmer, T. Fausett, P. Sadowski, and D. Whiteson, *Eur. Phys. J. C* **76**, 235 (2016), [arXiv:1601.07913 \[hep-ex\]](#).
  - [39] R. T. D’Agnolo and A. Wulzer, *Phys. Rev. D* **99**, 015014 (2019), [arXiv:1806.02350 \[hep-ph\]](#).
  - [40] J. H. Collins, K. Howe, and B. Nachman, *Phys. Rev. D* **99**, 014038 (2019), [arXiv:1902.02634 \[hep-ph\]](#).
  - [41] J. H. Collins, K. Howe, and B. Nachman, *Phys. Rev. Lett.* **121**, 241803 (2018), [arXiv:1805.02664 \[hep-ph\]](#).
  - [42] I. J. Goodfellow, J. Pouget-Abadie, M. Mirza, B. Xu, D. Warde-Farley, S. Ozair, A. Courville, and Y. Bengio, in *Proceedings of the 27th International Conference on Neural Information Processing Systems - Volume 2*, NIPS’14 (MIT Press, Cambridge, MA, USA, 2014) pp. 2672–2680.
  - [43] M. Zaheer, S. Kottur, S. Ravanbakhsh, B. Póczos, R. Salakhutdinov, and A. J. Smola, *CoRR abs/1703.06114* (2017), [arXiv:1703.06114](#).
  - [44] L. de Oliveira, M. Kagan, L. Mackey, B. Nachman, and A. Schwartzman, *JHEP* **07**, 069 (2016), [arXiv:1511.05190 \[hep-ph\]](#).
  - [45] P. Baldi, K. Bauer, C. Eng, P. Sadowski, and D. Whiteson, *Phys. Rev. D* **93**, 094034 (2016), [arXiv:1603.09349 \[hep-ex\]](#).
  - [46] J. Barnard, E. N. Dawe, M. J. Dolan, and N. Rajcic, *Phys. Rev. D* **95**, 014018 (2017), [arXiv:1609.00607 \[hep-ph\]](#).
  - [47] P. T. Komiske, E. M. Metodiev, and M. D. Schwartz, *JHEP* **01**, 110 (2017), [arXiv:1612.01551 \[hep-ph\]](#).
  - [48] G. Louppe, K. Cho, C. Becot, and K. Cranmer, *JHEP* **01**, 057 (2019), [arXiv:1702.00748 \[hep-ph\]](#).
  - [49] H. Qu and L. Gouskos, (2019), [arXiv:1902.08570 \[hep-ph\]](#).
  - [50] A. Butter, G. Kasieczka, T. Plehn, and M. Russell, *SciPost Phys.* **5**, 028 (2018), [arXiv:1707.08966 \[hep-ph\]](#).
  - [51] D. Guest, J. Collado, P. Baldi, S.-C. Hsu, G. Urban, and D. Whiteson, *Phys. Rev. D* **94**, 112002 (2016), [arXiv:1607.08633 \[hep-ex\]](#).
  - [52] ATLAS Collaboration, *ATL-PHYS-PUB-2017-003* (2017).
  - [53] CMS Collaboration, *CMS-DP-2017-049* (2017).
  - [54] A. M. Sirunyan *et al.* (CMS), *JINST* **13**, P05011 (2018), [arXiv:1712.07158 \[physics.ins-det\]](#).
  - [55] T. Sjöstrand, S. Ask, J. R. Christiansen, R. Corke, N. Desai, P. Ilten, S. Mrenna, S. Prestel, C. O. Rasmussen, and P. Z. Skands, *Comput. Phys. Commun.* **191**, 159 (2015), [arXiv:1410.3012 \[hep-ph\]](#).
  - [56] T. Sjöstrand, S. Mrenna, and P. Z. Skands, *JHEP* **05**, 026 (2006), [arXiv:hep-ph/0603175 \[hep-ph\]](#).
  - [57] M. Cacciari, G. P. Salam, and G. Soyez, *JHEP* **04**, 063 (2008), [arXiv:0802.1189 \[hep-ph\]](#).
  - [58] M. Cacciari, G. P. Salam, and G. Soyez, *Eur. Phys. J. C* **72**, 1896 (2012), [arXiv:1111.6097 \[hep-ph\]](#).
  - [59] M. Cacciari and G. P. Salam, *Phys. Lett. B* **641**, 57 (2006), [arXiv:hep-ph/0512210 \[hep-ph\]](#).
  - [60] P. Skands, S. Carrazza, and J. Rojo, *Eur. Phys. J. C* **74**, 3024 (2014), [arXiv:1404.5630 \[hep-ph\]](#).
  - [61] F. Chollet, “Keras,” <https://github.com/fchollet/keras> (2017).
  - [62] M. Abadi, P. Barham, J. Chen, Z. Chen, A. Davis, J. Dean, M. Devin, S. Ghemawat, G. Irving, M. Isard, *et al.*, in *OSDI*, Vol. 16 (2016) pp. 265–283.
  - [63] D. Kingma and J. Ba, (2014), [arXiv:1412.6980 \[cs\]](#).
  - [64] J. Thaler and K. Van Tilburg, *JHEP* **02**, 093 (2012), [arXiv:1108.2701 \[hep-ph\]](#).
  - [65] J. Thaler and K. Van Tilburg, *JHEP* **03**, 015 (2011), [arXiv:1011.2268 \[hep-ph\]](#).
  - [66] A. J. Larkoski, G. P. Salam, and J. Thaler, *JHEP* **06**, 108 (2013), [arXiv:1305.0007 \[hep-ph\]](#).
  - [67] A. Pathak, P. Komiske, E. Metodiev, and M. Schwartz, “Herwig7.1 quark and gluon jets,” (2019).
  - [68] P. Komiske, E. Metodiev, and J. Thaler, “Pythia8 quark and gluon jets for energy flow,” (2019).
  - [69] A. Badea, A. Baty, P. Chang, G. M. Innocenti, M. Maggi, C. McGinn, M. Peters, T.-A. Sheng, J. Thaler, and Y.-J. Lee, (2019), [arXiv:1906.00489 \[hep-ex\]](#).
  - [70] K. Cranmer, J. Pavez, and G. Louppe, (2015), [arXiv:1506.02169 \[stat.AP\]](#).

## Appendix A: Optimal Functions

The results presented here can be found (as exercises) in textbooks, but are repeated here for easy access. Let  $X$  be some discriminating features and  $Y \in \{0, 1\}$  is another random variable representing class membership.

Consider the general problem of minimizing some average loss for the function  $f(x)$ :

$$f = \operatorname{argmin}_{f'} \mathbb{E}[\operatorname{loss}(f'(X), Y)], \quad (\text{A1})$$

where  $\mathbb{E}$  means ‘expected value’, i.e. average value or mean (sometimes represented as  $\langle \cdot \rangle$ ). The expectation values are performed over the joint probability density of  $(X, Y)$ . One can rewrite Eq. A1 as

$$f = \operatorname{argmin}_{f'} \mathbb{E}[\mathbb{E}[\operatorname{loss}(f'(X), Y) | X]]. \quad (\text{A2})$$

The advantage<sup>2</sup> of writing the loss as in Eq. A2 is that one can see that it is sufficient to minimize the function (and not functional)  $\mathbb{E}[\operatorname{loss}(f'(x), Y) | X = x]$  for all  $x$ . To see this, let  $g(x) = \operatorname{argmin}_{f'} \mathbb{E}[\operatorname{loss}(f'(x), Y) | X = x]$  and suppose that  $h(x)$  is a function with a strictly smaller loss in Eq. A1 than  $g$ . Since the average loss for  $h$  is below that of  $g$ , by the intermediate value theorem, there must be an  $x$  for which the average loss for  $h$  is below that of  $g$ , contradicting the construction of  $g$ .

Now, consider the case where the loss is cross-entropy:

$$\max_z \mathbb{E}[Y \log(z) + (1 - Y) \log(1 - z) | X] \quad (\text{A3})$$

$$= \max_z (\mathbb{E}[Y | X] \log(z) + (1 - \mathbb{E}[Y | X]) \log(1 - z)), \quad (\text{A4})$$

where  $z = f'(x)$  is fixed. Equation A3 is maximized for  $g(x) = \mathbb{E}[Y | X = x]$ . Coincidentally, the exact same result holds if using mean squared error loss. When using either loss function with two outputs and the softmax activation for the last neural network layer, the first output will asymptotically approach  $g(x)$  and the other by construction will be  $1 - g(x)$ . The ratio of these two outputs is then:

$$\frac{g(x)}{1 - g(x)} = \frac{\mathbb{E}[Y | X = x]}{\mathbb{E}[1 - Y | X = x]} \quad (\text{A5})$$

$$= \frac{\Pr(Y = 1 | X = x)}{\Pr(Y = 0 | X = x)} \quad (\text{A6})$$

$$= \frac{p(X | Y = 1) \Pr(Y = 1)}{p(X | Y = 0) \Pr(Y = 0)} \quad (\text{A7})$$

$$= \text{Likelihood ratio} \times \frac{\Pr(Y = 1)}{\Pr(Y = 0)}. \quad (\text{A8})$$

Therefore, the output is proportional to the likelihood ratio. The proportionality constant is the ratio of fractions of the two classes used during the training. In the paper, the two classes always have the same number of examples and thus this factor is unity.

---

<sup>2</sup> The derivation below for the mean-squared error was partially

inspired by Appendix A in Ref. [70].